

Radiology Report Generation with a Learned Knowledge Base and Multi-modal Alignment

Shuxin Yang^{1,5}, Xian Wu³, Shen Ge³, Xingwang Wu⁴, S. Kevin Zhou^{1,2}, Li Xiao^{1,5}

¹The Key Lab of Intelligent Information Processing of Chinese Academy of Sciences (CAS), Institute of Computing Technology, CAS, Beijing, 100190, China

²School of Biomedical Engineering & Suzhou Institute for Advanced Research Center for Medical Imaging, Robotics, and Analytic Computing & LEarning (MIRACLE) University of Science and Technology of China, Suzhou 215123, China

³Tencent Medical AI Lab, Beijing, 100094, China

⁴The First Affiliated Hospital of Anhui Medical University, HeFei, 230022, China

⁵University of Chinese Academy of Sciences, Beijing, 100049, China

Abstract

In clinics, a radiology report is crucial for guiding a patient's treatment. Unfortunately, report writing imposes a heavy burden on radiologists. To effectively reduce such a burden, we hereby present an automatic, multi-modal approach for report generation from chest x-ray. Our approach, motivated by the observation that the descriptions in radiology reports are highly correlated with the x-ray images, features two distinct modules: (i) *Learned knowledge base*. To absorb the knowledge embedded in the above-mentioned correlation, we automatically build a knowledge base based on textual embedding. (ii) *Multi-modal alignment*. To promote the semantic alignment among reports, disease labels and images, we explicitly utilize textual embedding to guide the learning of the visual feature space. We evaluate the performance of the proposed model using metrics from both natural language generation and clinic efficacy on the public IU and MIMIC-CXR datasets. Our ablation study shows that each module contributes to improving the quality of generated reports. Furthermore, with the aid of both modules, our approach clearly outperforms state-of-the-art methods.

Introduction

The radiology report is crucial for assisting clinic decision making (Zhou, Rueckert, and Fichtinger 2019). It describes some observations on images such as diseases' degree, size, and location. However, the process of writing reports is time-consuming and tedious for radiologists (Bruno, Walker, and Abujudeh 2015). With the advancement of deep learning and natural language processing, automatic radiology report generation has attracted growing research interests.

Many radiology report generation approaches follow the practice of image captioning models (Xu et al. 2015; Lu et al. 2017; Anderson et al. 2018). For example, (Jing, Xie, and Xing 2018; Yuan et al. 2019) employ the encoder-decoder architecture and propose the hierarchical generator as well as the attention mechanism to generate long reports. However, radiology report generation task is different from image captioning task. In image captioning, the model is required to cover the details of the input image, while for radiology report generation, the model is required to focus on the abnormal regions and infer potential diseases. Therefore, to

generate a correct radiology report, the model needs to identify the abnormal regions and provide proper descriptions. To this end, the medical background knowledge needs to be included in modeling.

Recently, some works attempt to integrate medical knowledge in modeling: MKG (Zhang et al. 2020) and PPKED (Liu et al. 2021) incorporate manual pre-constructed knowledge graphs to enhance the generation, HRGR (Li et al. 2018) builds a template database based on prior knowledge by manually filtering a set of sentences in the training corpus. These methods achieve improved performance over image captioning models. However, these models need to build the knowledge graph or template database in advance which is still laborious. In addition, when applying these models to images of other diseases, the knowledge graph or template database needs to be updated as well.

In this paper, we propose a knowledge base updating mechanism to store medical knowledge automatically. It learns a knowledge base from training data. Firstly, we initialize a memory as a knowledge base and use CNN/BERT model to extract visual features and textual embeddings from the input images and corresponding reference reports. Next, the knowledge base is updated by the report embeddings during the training phase. At the end of training, we fix the knowledge base as the model's parameter and use it for report generation. To acquire the related knowledge of the input image, we propose a visual-knowledge attention module that queries knowledge base with visual features. Finally, we employ the standard Transformer model with the help of the visual features and acquired knowledge to generate radiology reports.

Since the critical clinical information usually comes from descriptions of abnormalities, where such sentences are rare and diverse in radiology datasets, we need to enable the knowledge base to focus on the knowledge of abnormalities. To this end, we propose a multi-modal alignment mechanism. It consists of visual-textual alignment and visual-label alignment. The intuition is that the reports and disease labels describe the same observations on the images, so the semantic features among images, reports, and disease labels should be consistent. Specifically, we adapt the triplet margin loss (Balntas et al. 2016) to align the visual features and

textual embeddings, as well as the binary cross-entropy loss to align the visual features and disease labels. Guided by the proposed multi-modal alignment, the proposed knowledge base can store the knowledge of abnormalities which works together with the visual encoder to generate accurate descriptions of abnormalities.

We evaluate our proposed methods on the publicly accessible IU and MIMIC-CXR datasets. Besides natural language generation (NLG) metrics, we adopt clinical efficacy (CE) metrics to analyze the quality of generation reports in clinics. The results show that the proposed method achieves state-of-the-art performance on NLG and CE metrics. It also indicates that the radiology report generation benefits from the multi-modal alignment mechanism and the learned knowledge base, avoiding laborious manual construction. Furthermore, the proposed methods boost the quality of generated reports in both language and clinical correctness.

The main contributions are as follows:

- We propose a novel radiology generation framework with a knowledge base, which could be learned automatically from the training data by a novel updating mechanism.
- We propose a multi-modal alignment mechanism that promotes the semantic alignment among images, reports, and disease labels to guide the learning of visual features.
- Our experiments demonstrate consistent performance improvements of our proposed methods. Furthermore, our model achieves state-of-the-art performance on various metrics for both the public IU and MIMIC-CXR datasets.

Related Work

With the advancement of computer vision and natural language processing, many works exploit to combine radiology images and free-text for automatically generating reports to assist radiologists in the clinic (Zhou et al. 2021). Inspired by image captioning, (Shin et al. 2016) adopts the CNN-RNN framework to describe the detected diseases based on visual features on a chest x-ray dataset. The work is restricted to the categories of predefined diseases. The Co-Att (Jing, Xie, and Xing 2018) and (Xue et al. 2018; Yuan et al. 2019) propose different attention mechanisms and hierarchical LSTM to generate radiology reports. However, most reports generated by such works tend to describe normal observations, which indicates that such methods have difficulties in capturing subtle changes in the image. Our proposed method is similar to the TieNet (Wang et al. 2018) which proposes an attention encoded text embedding and a saliency weighted global average pooling to boost the image classification and report generation. However, the method uses the report embeddings as a part of LSTM’s input which is not available in the inference stage, resulting in embedding bias in the report generation. Other types of work explore injecting extra prior knowledge into the generation model to improve the quality of the generated radiology reports. Following the writing practice of radiologists, the HRGR (Li et al. 2018) compiles a manually extracted template database to generate radiology reports by reinforcement learning. The KERP (Li et al. 2019), MKG (Zhang et al. 2020) and PPKED (Liu et al. 2021)

propose to combine pre-constructed knowledge graph for radiology report generation. Although these methods achieved remarkable results, building the template database and knowledge graph is still laborious, making it hard to transfer those approaches directly to other datasets. In this paper, we propose a knowledge-enhancing generator without manual labor to build a knowledge base.

As revealed by recent studies (Graves et al. 2016; Wu et al. 2018; Chen et al. 2020a), the memory mechanism can provide prior knowledge to boost the generation model. The R2Gen (Chen et al. 2020b) proposes a relational memory in the decoder to learn the order of words or sentences. Nevertheless, the order relies on the radiologist’s personal style. The KVMN (Miller et al. 2016) proposes a key-value structured memory that automatically encodes prior knowledge into the memory for question and answer tasks (QA). Our work is different from KVMN in three aspects. First, KVMN deals with a different task (QA) which is a classification problem. As a result, their framework cannot be directly applied to medical report generation. Second, the knowledge source of KVMN is pre-defined by a manually prepared database, while our knowledge base is learned from scratch during training. Third, we propose a multi-head updating mechanism that has more expressive ability than the KVMN model.

Method

In this section, we introduce the proposed method. Firstly, we provide the notation and formulate the radiology report generation task; Secondly, we propose the framework of our method; Thirdly, we describe the proposed knowledge base updating and multi-modal alignment mechanism in detail.

Notation and Problem Formulation

Let Img denote a radiology image, $\mathbf{Y} = \{y_1, \dots, y_{N_L} | y_i = 0/1\}$ denote the class label of this image, $\mathbf{W}^* = \{w_1^*, w_2^*, \dots, w_{N_R}^* | w_i^* \in \mathbb{V}\}$ denote the reference report, $\mathbf{W} = \{w_1, w_2, \dots, w_{N_W} | w_i \in \mathbb{V}\}$ denote the report generated by the model. Here w_i^* and w_i refer to the index of word in vocabulary \mathbb{V} , N_L is the number of labels, N_R and N_W are the length of the reference and generated reports. In the training stage of the proposed model, we need Img , \mathbf{Y} and \mathbf{W}^* ; In the testing stage, we only need Img to generate \mathbf{W} .

Framework

Figure 1 displays the framework of the proposed model: a knowledge-enhancing generator, a knowledge-updating module, and a multi-modal alignment module. All three modules are used in the training stage, and only the knowledge-enhancing generator is used in the testing stage. In training, the knowledge-updating module and the multi-modal alignment module work together to restore learned knowledge into the knowledge base; In prediction, the knowledge base is fixed. The knowledge-enhancing generator extracts related knowledge from the knowledge base to generate radiology reports.

Firstly, we extract visual features from the input radiology image. Following previous works (Jing, Xie, and Xing 2018; Wang et al. 2018; Chen et al. 2020b), the convolution neural

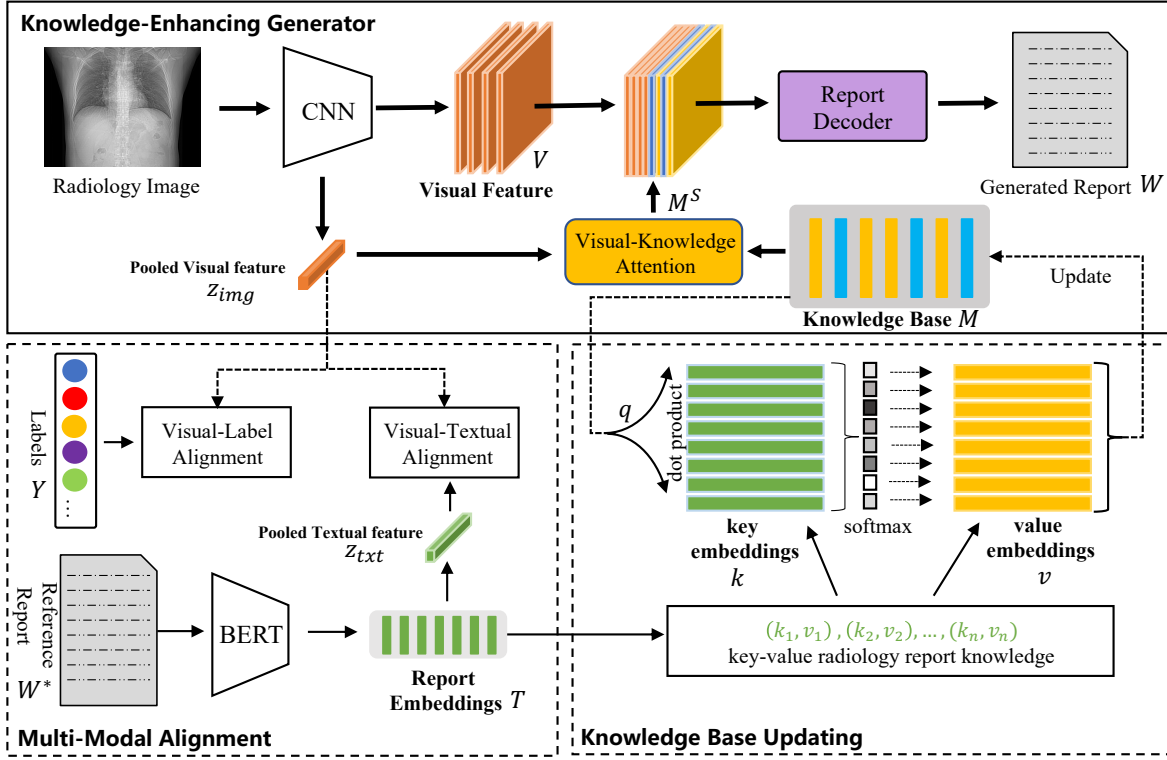


Figure 1: The architecture of the proposed model during training stage. The dashes lines and boxes are only used to learn the knowledge base and optimize multi-modal semantic alignment.

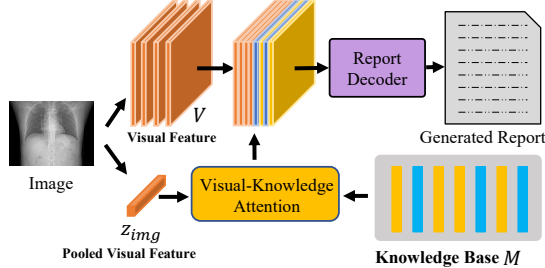


Figure 2: The architecture of the proposed model during inference stage. The visual encoder is omitted because of limited space.

network (CNN) is employed as our visual encoder, and the visual features are extracted from the last convolution layer:

$$\mathbf{V} = \text{CNN}(\text{Img})W^E, \quad (1)$$

where W^E are learnable parameters for affine transformation, $\mathbf{V} \in \mathbb{R}^{K \times D}$ represents the extracted visual features, where K and D denote the number of the visual features and the dimension of each feature, respectively.

Next, we acquire the aggregated visual features by average pooling:

$$\mathbf{z}_{img} = \text{AveragePooling}(\mathbf{V}), \quad (2)$$

where \mathbf{z}_{img} has the dimension of D .

During training, we also extract report embeddings from reference reports to update the knowledge base and guide the learning of visual features. Similar to BERT model (Devlin et al. 2019), we employ the encoder of Transformer (Vaswani et al. 2017) as our report encoder to extract report embeddings. The report embeddings are acquired from the hidden states of the last layer:

$$\mathbf{T} = \text{BERT}(\mathbf{W}^*), \quad (3)$$

where \mathbf{W}^* denotes the reference reports written by radiologists, $\text{BERT}(\cdot)$ refers to the report encoder, and $\mathbf{T} \in \mathbb{R}^{N_R \times D}$ is extracted textual embedding.

In BERT, the first token (CLS) of a sentence is regarded as the aggregate representation of the entire sequence. Based on the report embedding acquired in Eq.(3), the aggregated textual feature of the report \mathbf{z}_{txt} is acquired by Eq.(4).

$$\mathbf{z}_{txt} = \mathbf{T}_{[CLS]}W^Z + b^Z \quad (4)$$

where $\mathbf{T}_{[CLS]}$ denotes the embedding of CLS in report embeddings \mathbf{T} , W^Z is a learnable affine transformation, and b^Z is a bias. Thus, \mathbf{z}_{txt} has the dimension of D .

Knowledge Base Updating

Different from image captioning, radiology report generation requires professional medical domain knowledge. The radiologists need to examine diseases' degree, size, and location before writing reports. To distill the domain knowledge

conceived in the pairs of radiology images, we introduce the memory mechanism. As revealed by recent studies (Graves et al. 2016; Wu et al. 2018; Chen et al. 2020a), the memory mechanism can provide prior knowledge to boost the generation model. Inspired by this, we initialize a memory as a radiology knowledge base and propose an updating mechanism to learn from training data.

In our implementation, we use a matrix to initialize the knowledge base $\mathbf{M}_0 \in \mathbb{R}^{N_m \times D}$, where N_m is the base size and D is the dimension. In initialization, the diagonal element of \mathbf{M}_0 is set 1, and other elements are set to 0.

To model the relationship among the knowledge base, the textual features from the reference reports, and the visual features from input images, we use the multi-head attention (MHA) (Vaswani et al. 2017) mechanism. The MHA consists of n parallel heads and each head is defined as a scaled dot-product attention:

$$\text{Att}_i(X, Y) = \text{softmax} \left(\frac{X \mathbf{W}_i^Q (Y \mathbf{W}_i^K)^T}{\sqrt{d_n}} \right) Y \mathbf{W}_i^V$$

$$\text{MHA}(X, Y) = [\text{Att}_1(X, Y); \dots; \text{Att}_n(X, Y)] \mathbf{W}^O \quad (5)$$

where $X \in \mathbb{R}^{l_x \times d}$ and $Y \in \mathbb{R}^{l_y \times d}$ denote the Query matrix and the Key/Value matrix, respectively; $\mathbf{W}_i^Q, \mathbf{W}_i^K, \mathbf{W}_i^V \in \mathbb{R}^{d \times d_n}$ and $\mathbf{W}^O \in \mathbb{R}^{d \times d}$ are learnable parameters, where $d_n = d/n$. $[\cdot; \cdot]$ stands for concatenation operation.

To update the knowledge base \mathbf{M}_{t-1} at the training step $t-1$, we use the textual features extracted from the reference reports identifying the knowledge that is missing in \mathbf{M}_{t-1} .

$$\Delta \mathbf{M}_t = \text{MHA}(\mathbf{M}_{t-1}, \mathbf{T}) \quad (6)$$

where $\Delta \mathbf{M}_t$ stands for the incremental knowledge acquired at the training step t and \mathbf{T} denotes the textual features acquired in Eq.(3). By integrating the incremental knowledge, we can acquire the updated knowledge base at training step t .

$$\mathbf{M}_t = \mathbf{M}_{t-1} + \text{Norm}(\Delta \mathbf{M}_t) \quad (7)$$

where *Norm* refers to layer normalization to normalize the incremental knowledge.

Next, we acquire supporting knowledge regarding the current image by multi-head attention.

$$\mathbf{M}^S = \text{MHA}(\mathbf{z}_{img}, \mathbf{M}_t) \quad (8)$$

where \mathbf{M}^S refers to the supporting knowledge, \mathbf{z}_{img} refers to the pooled visual feature acquired from Eq.(2).

The report generator automatically generates a medical report using visual features and the learned knowledge base. The Transformer-based model has proven effective in natural language processing (Devlin et al. 2019). Thus, we employ a standard Transformer model as our report generator (Vaswani et al. 2017) which includes a stack of self-attention layers and masked self-attention layers. The generator decodes the concatenation of visual features and the supporting knowledge to a sequence of hidden representation and follows the auto-regressive decoding process generating the radiology report \mathbf{W} from the conditional distribution:

$$p_\theta(\mathbf{W} | [\mathbf{V}; \mathbf{M}^S]) = \prod_{t=1}^{N_W} p_\theta(w_t | w_{<t}, [\mathbf{V}; \mathbf{M}^S]), \quad (9)$$

where θ refers to the model's parameters, $w_{<t}$ denotes the generated words before time step t , and \mathbf{V} refers to visual features acquired in Eq.(1).

Multi-Modal Alignment

In this section, we introduce the Multi-Modal Alignment module which aligns the visual, textual, and disease labels to guide the learning of the proposed model.

Textual-Textual Alignment. Following the paradigm of natural language generation, our basic model maximizes the likelihood of generated reports by minimizing the cross-entropy loss. The model is optimized by the consistency between generated and reference reports, so we named it textual-textual (T-T) alignment.

$$\mathcal{L}_{T-T} = -\frac{1}{N_W} \sum_{i=0}^{N_W} \log p_\theta(\mathbf{W} | [\mathbf{V}; \mathbf{M}^S]) \quad (10)$$

where \mathbf{W} is the generated sequence.

Besides the general textual-textual alignment, we propose two extra multi-modal alignments. The radiology report generation is a multi-modal task that aims to transform radiology images into reports. Since reports and disease labels describe the observations on the x-ray image, the semantic features among images, reports, and disease labels should be consistent. Following this intuition, we proposed *visual-textual (V-T) alignment* and *visual-label (V-L) alignment* to encourage our model to be consistent among different modalities and guide the learning of the proposed model.

Visual-Textual Alignment The visual-textual alignment module tries to make the features in radiology images and reference reports to be close. Firstly, we extract the pooled textual feature \mathbf{z}_{txt} from the reference report and the pooled visual features \mathbf{z}_{img} from the input image. As illustrated in (Chauhan et al. 2020), the triplet margin loss (Balntas et al. 2016) model performs well for joining image learning and report in the radiology image classification task. We adapt the image-to-text and text-to-image triplet margin loss losses which force the paired features closer than unpaired features in latent space. This helps to model the bidirectional inter-relationship between image and report. Given a target pair $\{\mathbf{z}_{img}, \mathbf{z}_{txt}\}$, we sample a negative pair $\{\mathbf{z}_{img}^{(n)}, \mathbf{z}_{txt}^{(n)}\}$ from the training set, and the visual-textual alignment is formulated as:

$$\mathcal{L}_{V-T} = \max(0, \mu + d(\mathbf{z}_{img}, \mathbf{z}_{txt}) - d(\mathbf{z}_{img}, \mathbf{z}_{img}^{(n)}))$$

$$+ \max(0, \mu + d(\mathbf{z}_{txt}, \mathbf{z}_{img}) - d(\mathbf{z}_{txt}, \mathbf{z}_{txt}^{(n)})) \quad (11)$$

$$\text{where } d(\mathbf{z}_1, \mathbf{z}_2) = 1 - \frac{\mathbf{z}_1 \cdot \mathbf{z}_2}{\|\mathbf{z}_1\| \cdot \|\mathbf{z}_2\|} \quad (12)$$

$$L = \max(0, \mu + d(\mathbf{z}_{img}, \mathbf{z}_{txt}) - d(\mathbf{z}_{img}, \mathbf{z}_{img}^{(n)})) \quad (13)$$

In our implementation, $d(\cdot, \cdot)$ is a distance function to quantify the closeness of two modalities, and μ is a margin parameter defined as Eq.(14), which is determined by the difference of disease labels between the target image and negative image.

$$\mu = \begin{cases} 0 & \mathbf{Y} = \mathbf{Y}^{(n)} \\ \max(0.5, \frac{1}{N_L} \sum_i^{N_L} |y_i - y_i^{(n)}|) & \mathbf{Y} \neq \mathbf{Y}^{(n)} \end{cases} \quad (14)$$

Table 1: The performances of our model compared with baselines on IU and MIMIC-CXR datasets. The best results are highlighted in bold. For the baselines marked by *, we cite the results reported in (Jing, Wang, and Xing 2019). For the baselines marked by #, we replicate results by their codes; the rests are cited from the original paper.

Dataset	Model	BLEU-1	BLEU-2	BLEU-3	BLEU-4	CIDEr	ROUGE-L
IU	S&T*	0.216	0.124	0.087	0.066	0.294	0.306
	SA&T#	0.399	0.251	0.168	0.118	0.302	0.323
	AdaAtt*	0.220	0.127	0.089	0.068	0.295	0.308
	CMAS*	0.464	0.301	0.210	0.154	0.275	0.362
	KERP	0.482	0.325	0.226	0.162	0.280	0.339
	R2Gen	0.470	0.304	0.219	0.165	/	0.371
	PPKED	0.483	0.315	0.224	0.168	0.351	0.376
	Our	0.497	0.319	0.230	0.174	0.407	0.399
MIMIC-CXR	S&T#	0.256	0.157	0.102	0.070	0.063	0.249
	SA&T#	0.304	0.177	0.112	0.077	0.083	0.249
	AdaAtt#	0.311	0.178	0.111	0.075	0.084	0.246
	TopDown#	0.280	0.169	0.108	0.074	0.073	0.250
	R2Gen	0.353	0.218	0.145	0.103	/	0.277
	PPKED	0.360	0.224	0.149	0.106	/	0.284
	Our	0.386	0.237	0.157	0.111	0.111	0.274

where $\mathbf{Y} \in \mathbb{R}^{N_L}$ and $\mathbf{Y}^{(n)} \in \mathbb{R}^{N_L}$ denote the disease labels of input image and negative sampled image, respectively.

Visual-Label Alignment. Let $\mathbf{Y}' \in \mathbb{R}^{N_L}$ denote the predicted labels of current input image by the proposed model. Then the visual-label alignment is calculated as follows.

$$\mathbf{Y}' = \mathbf{z}_{img} W^L + b^L \quad (15)$$

where W^L is a learn-able affine transformation, and b^L is a bias.

Next, we adopt binary cross entropy loss to optimize the model on the consistency between visual and disease labels:

$$\mathcal{L}_{V-L} = -\frac{1}{N_L} \sum_{i=0}^{N_L} y_i \log \phi(y'_i) \quad (16)$$

where y_i and y'_i are ground-truth label and the predicted label in Eq.(15), respectively, and $\phi(\cdot)$ denotes a sigmoid function.

Finally, we optimize the proposed model with the textual-textual alignment \mathcal{L}_{T-T} , the visual-textual alignment \mathcal{L}_{V-T} , and the visual-label alignment \mathcal{L}_{V-L} . It is formulated as:

$$\mathcal{L} = \lambda_1 \mathcal{L}_{T-T} + \lambda_2 \mathcal{L}_{V-T} + \lambda_3 \mathcal{L}_{V-L}, \quad (17)$$

where λ_1 , λ_2 , and λ_3 are coefficients to balance the three constraint terms.

Experiment

In this section, we evaluate the proposed model on MIMIC-CXR and IU datasets and conduct some ablation studies to analyze the performance of the proposed model and the effectiveness of each component.

Dataset

MIMIC-CXR. MIMIC-CXR (Johnson et al. 2019) is a large dataset that contains 377,110 chest x-ray images and 227,827 free-text radiology reports associated with these images for 65,379 patients. The dataset contains multi-view images, and we filter frontal and lateral view images following previous works (Chen et al. 2020b). The dataset is labeled for 14 common chest radiology observations derived from the free-text radiology reports by a label tool CheXpert (Irvin et al. 2019).

IU. Indiana University Chest X-ray Collection (Demner-Fushman et al. 2016) is a public radiology examination dataset containing 3,955 radiology reports and 7,470 posterior-anterior/lateral view chest x-ray images. Each report consists of MeSH, indication, comparison, findings, and impression. For consistency, we employ the CheXpert to extract the labels as to the IU dataset.

The finding section in both datasets is used as the ground-truth reference report since it directly describes the observations on x-ray images. First, we filter out the reports without x-ray images or images missing findings section. Then, each report is converted to lower case and filtered out with a minimum frequency of three, which results in 760/7866 unique words on IU and MIMIC-CXR datasets, respectively. The labels include 12 disease labels and 2 individual labels indicating "No finding" and "Support device". There is no official split of the dataset for the IU dataset, so we follow the data split of previous SOTA work R2Gen (Chen et al. 2020b) which splits the data into training, validation, and testing set using a ratio 7:1:2 without overlap in patients. For the MIMIC-CXR dataset, the official split is adopted.

Implementation Detail

In our implementation, we employ the ResNet-101 (He et al. 2016) model as our visual encoder pre-trained on ImageNet. The report encoder and generator are implemented by ourselves and trained from scratch. All hyper-parameters are selected by the performances on the validation set. The layer of report encoder is set to 3. The dimension of the model is set to 512. All images are resized to 224×224 , and we use zero-padding for each mini-batch reports to keep the same length. Except for the visual encoder with an initial learning rate of $5e-5$, we use the Adam optimizer with an initial learning rate of $1e-4$ and weight decay of $5e-5$ for training. We train the model with epochs of 50 and 30 for the IU and MIMIC-CXR datasets, respectively. The coefficients of multi-modal alignment λ_1 , λ_2 , and λ_3 are set to 1, 0.1, and 0.1. We evaluate the proposed model on the validation set and report the test set results when the performance of the validation set achieves the best BLEU-4 score.

Quantitative Results

We adopt the widely used NLG metrics and clinical efficacy metrics to evaluate the performance of the proposed model. The NLG metrics include BLEU-n (Papineni et al. 2002), CIDEr (Vedantam, Lawrence Zitnick, and Parikh 2015), and ROUGE-L (Lin 2004) score. We compute these metrics using MSCOCO caption evaluation tool¹. The clinical efficacy (CE) metrics are proposed in R2Gen (Chen et al. 2020b), including precision, recall, and F1 score of the disease labels described in reference and generated radiology reports. Since the IU dataset does not provide consistent labels, we only report CE metrics on the MIMIC-CXR dataset. For consistency, we employ the CheXpert to extract the labels from generated reports.

We compare our proposed model with general image captioning works, e.g., **S&T** (Vinyals et al. 2015), **SA&T** (Xu et al. 2015), **AdaAtt** (Lu et al. 2017), and **TopDown** (Anderson et al. 2018), and specific medical report generation works, e.g., **CMAS** (Jing, Wang, and Xing 2019), **KERP** (Li et al. 2019), **R2Gen** (Chen et al. 2020b), and **PPKED** (Liu et al. 2021).

Table 2: The results of clinical efficacy metrics on the MIMIC-CXR dataset. The ACC, P, R, F1 denote accuracy, precision, recall, and F1 score, respectively.

Model	ACC	P	R	F1
S&T	0.423	0.084	0.066	0.072
SA&T	0.703	0.181	0.134	0.144
AdaAtt	0.741	0.265	0.178	0.197
TopDown	0.743	0.166	0.121	0.133
R2Gen	/	0.333	0.273	0.276
Ours	0.795	0.420	0.339	0.352

The NLG and CE results are shown in Table 1 and Table 2, respectively. First, as we can see from the NLG results, our

¹<https://github.com/tylin/coco-caption>

proposed method outperforms almost previous works except for slightly lower Rouge-L score on the MIMIC-CXR dataset and BLEU-2 score on the IU dataset. The results prove the effectiveness of the proposed method for radiology report generation. Second, in terms of CE metrics, our method remarkably outperforms the previous works, which indicates that our model generates more accurate reports than others in clinics. The potential reason for this might come from two aspects. On the one hand, guided by the reference reports and disease labels in training via semantic alignment, the visual feature space is better learned. On the other hand, the learned knowledge base can provide useful knowledge about observations on radiology images.

Ablation Study

We conduct experiments to analyze the effectiveness of the multi-modal alignment mechanism and the impact of the knowledge base size.

Table 3: The performance of different alignments on both datasets. The V-T and V-L refer to visual-textual alignment and visual-label alignment, respectively.

Dataset	Alignment	BLUE-3	BLUE-4	ROUGE-L
IU	-	0.207	0.157	0.356
	V-L	0.215	0.163	0.371
	V-T	0.221	0.162	0.382
	V-T + V-L	0.230	0.174	0.399
MIMIC	-	0.141	0.099	0.270
	V-L	0.149	0.105	0.271
	V-T	0.144	0.102	0.274
	V-T + V-L	0.157	0.111	0.274

Table 3 shows the performances of our model using different alignments on both datasets. The first three rows show that our model benefits from any alignment, which proves the effectiveness of the proposed two alignments. Furthermore, the model that combines two alignments achieves the best performance. This indicates that the alignments enforcing among different modalities in the model can boost the quality of radiology reports.

Table 4: The performance of different head size in knowledge base updating. *#Head* refers to the size of head. The BL-n, CDr, and RG-L denote BLEU-n, CIDEr, and ROUGE-L scores, respectively.

Dataset	#Head	BL-3	BL-4	CDr	RG-L
IU	1	0.205	0.149	0.289	0.372
	2	0.216	0.158	0.379	0.379
	4	0.225	0.164	0.371	0.379
	8	0.230	0.174	0.407	0.399
MIMIC	1	0.131	0.090	0.109	0.259
	2	0.144	0.101	0.103	0.271
	4	0.149	0.105	0.120	0.271
	8	0.157	0.111	0.111	0.274



X-ray image	Reference report	Our proposed method	Basic model
	<u>the endotracheal tube is in unchanged position</u> the nasogastric tube and the right central venous access line are also unchanged there are bilaterally increasing pleural effusions with subsequent increasing areas of basal atelectasis the overall lung volumes remain low moderate cardiomegaly is unchanged known pulmonary metastatic disease	there is no relevant change <u>the monitoring and support devices are in constant position</u> the lung volumes remain low there is unchanged evidence of bilateral pleural effusions with subsequent areas of atelectasis at the lung bases the size of the cardiac silhouette is unchanged unchanged appearance of the right lung	there is no relevant change <u>the monitoring and support devices are in constant position</u> constant appearance of the lung parenchyma and of the cardiac silhouette
	<u>the monitoring and support devices including the esophageal stent and the right-sided pigtail catheter are unchanged</u> the extensive known parenchymal opacities on the left and on the right are unchanged in extent and severity there is no evidence of newly occurred focal parenchymal opacity unchanged right pleural effusion no left pleural effusion unchanged size of the cardiac silhouette	there is no relevant change <u>the monitoring and support devices are in constant position</u> there is no evidence of pneumothorax the lung volumes remain low there is unchanged evidence of extensive bilateral parenchymal opacities the presence of a minimal left pleural effusion cannot be excluded unchanged appearance of the cardiac silhouette	the patient has received a nasogastric tube the course of the tube is unremarkable the tip of the tube projects over the middle parts of the stomach there is no evidence of complications notably no pneumothorax otherwise the radiograph is unchanged

Figure 3: Visualization of two samples with reports from the MIMIC-CXR dataset. The same color highlights the descriptions of the same disease. The descriptions of the support device are highlighted by underline.

To validate the impact of head size in knowledge base updating, we conduct experiments to evaluate the performance of models with different head sizes. As shown in Table 4, as the number of heads increases, the model’s performance improves consistently, showing enhanced expressive ability of using the multi-head mechanism to learn the features from different subspaces.

Table 5: The performance of our model with different size of knowledge bases. The #KB denotes the size of knowledge base, where 0 refers to the model without knowledge base. The BL-n, CDr, and RG-L denote BLEU-n, CIDEr, and ROUGE-L scores, respectively.

Dataset	#KB	BL-3	BL-4	CDr	RG-L
IU	0	0.197	0.149	0.366	0.376
	1	0.206	0.154	0.386	0.371
	10	0.211	0.155	0.375	0.368
	30	0.230	0.174	0.407	0.399
	60	0.227	0.173	0.416	0.395
MIMIC	0	0.126	0.091	0.104	0.269
	1	0.138	0.092	0.109	0.267
	10	0.148	0.104	0.106	0.270
	30	0.152	0.107	0.108	0.272
	60	0.157	0.111	0.111	0.274

The size of the knowledge base determines the capacity of the knowledge learning from reference reports. We train five models with sizes of 0, 1, 10, 30, and 60, where 0 means not using the knowledge base. As shown in Table 5, the performance of our model goes up as the size rises, but it achieves the best when the size is 30 on the IU dataset. The potential reason is that the IU dataset is relatively small, so the diversity is limited. As the size goes up, the redundant in-

formation stored may distract the model, leading to declined performance. The performance improves continuously on the MIMIC-CXR dataset, showing that the model benefits from the large knowledge base on a large dataset.

Qualitative Results

In Figure 3, we visualize two images with reports. Compared with the basic model, our model generates more accurate descriptions from the x-ray image. For example, in the first row, our model generates the descriptions of *pleural effusions*, *atelectasis*, and *cardiomegaly*, while the basic model lacks the key descriptions of *pleural effusions*, *atelectasis*. The potential reason may be the guiding of the multi-modal alignment mechanism, which helps the model better learn visual feature space and capture the subtle changes in radiology images. Furthermore, as we can see, our model outputs the descriptions with support devices with the same sentence “*the monitoring and support devices are in constant position*”, which are confirmed by the underlined sentences in the ground truth reports with similar meanings. However, the basic model only correctly describes the support device in the first row while omitting it in the second row. This clearly demonstrates the superiority of our model to use the knowledge base to learn a template representation from training reports about *support devices*, showing the advantage of report generation through utilizing a learned knowledge base.

Conclusion

We proposed a knowledge augment generation model with an automatic knowledge base and a semantic consistency mechanism for radiology report generation. We conducted experiments to validate the proposed model and demonstrated the effectiveness of each component on IU and MIMIC-CXR datasets. The results show that our model achieves state-of-the-art performances in terms of NLG and CE metrics on both

datasets. The ablation studies show that our model learns visual features well guided by semantic consistency constraints. Besides, the model benefits from the large size of the knowledge base on a large dataset. The proposed knowledge base updating method is easily applied to other datasets without extra labor, such as constructing a template database. In the future, we will apply the method to other generation systems.

References

- Anderson, P.; He, X.; Buehler, C.; Teney, D.; Johnson, M.; Gould, S.; and Zhang, L. 2018. Bottom-Up and Top-Down Attention for Image Captioning and VQA. In *CVPR*.
- Balntas, V.; Riba, E.; Ponsa, D.; and Mikolajczyk, K. 2016. Learning local feature descriptors with triplets and shallow convolutional neural networks. *British Machine Vision Conference 2016, BMVC 2016*, 2016-Sept: 119.1–119.11.
- Bruno, M. A.; Walker, E. A.; and Abujudeh, H. H. 2015. Understanding and confronting our mistakes: the epidemiology of error in radiology and strategies for error reduction. *Radiographics*, 35(6): 1668–1676.
- Chauhan, G.; Liao, R.; Wells, W.; Andreas, J.; Wang, X.; Berkowitz, S.; Horng, S.; Szolovits, P.; and Golland, P. 2020. Joint Modeling of Chest Radiographs and Radiology Reports for Pulmonary Edema Assessment. In *MICCAI 2020*, volume 12262 LNCS, 529–539. ISBN 9783030597122.
- Chen, X.; Fan, H.; Girshick, R.; and He, K. 2020a. Improved baselines with momentum contrastive learning. *arXiv*, 1–3.
- Chen, Z.; Song, Y.; Chang, T.-h.; and Wan, X. 2020b. Generating Radiology Reports via Memory-driven Transformer. In *Proceedings of the 2020 Conference on Empirical Methods in Natural Language Processing (EMNLP)*, 1439–1449. Association for Computational Linguistics.
- Demner-Fushman, D.; Kohli, M. D.; Rosenman, M. B.; Shooshan, S. E.; Rodriguez, L.; Antani, S.; Thoma, G. R.; and McDonald, C. J. 2016. Preparing a collection of radiology examinations for distribution and retrieval. *Journal of the American Medical Informatics Association*, 23(2): 304–310.
- Devlin, J.; Chang, M. W.; Lee, K.; and Toutanova, K. 2019. BERT: Pre-training of deep bidirectional transformers for language understanding. In *NAACL HLT 2019 - 2019 Conference of the North American Chapter of the Association for Computational Linguistics: Human Language Technologies - Proceedings of the Conference*, volume 1, 4171–4186. ISBN 9781950737130.
- Graves, A.; Wayne, G.; Reynolds, M.; Harley, T.; Danihelka, I.; Grabska-Barwińska, A.; Colmenarejo, S. G.; Grefenstette, E.; Ramalho, T.; Agapiou, J.; Badia, A. P.; Hermann, K. M.; Zwols, Y.; Ostrovski, G.; Cain, A.; King, H.; Summerfield, C.; Blunsom, P.; Kavukcuoglu, K.; and Hassabis, D. 2016. Hybrid computing using a neural network with dynamic external memory. *Nature*, 538(7626): 471–476.
- He, K.; Zhang, X.; Ren, S.; and Sun, J. 2016. Deep residual learning for image recognition. *Proceedings of the IEEE Computer Society Conference on Computer Vision and Pattern Recognition*, 2016-December: 770–778.
- Irvin, J.; Rajpurkar, P.; Ko, M.; Yu, Y.; Ciurea-Illcus, S.; Chute, C.; Marklund, H.; Haghighi, B.; Ball, R.; Shpanskaya, K.; Seekins, J.; Mong, D. A.; Halabi, S. S.; Sandberg, J. K.; Jones, R.; Larson, D. B.; Langlotz, C. P.; Patel, B. N.; Lungren, M. P.; and Ng, A. Y. 2019. CheXpert: A large chest radiograph dataset with uncertainty labels and expert comparison. *arXiv*.
- Jing, B.; Wang, Z.; and Xing, E. 2019. Show, Describe and Conclude: On Exploiting the Structure Information of Chest X-ray Reports. In *Proceedings of the 57th Annual Meeting of the Association for Computational Linguistics*, 6570–6580. Association for Computational Linguistics. ISBN 9781950737482.
- Jing, B.; Xie, P.; and Xing, E. 2018. On the Automatic Generation of Medical Imaging Reports. In *Proceedings of the 56th Annual Meeting of the Association for Computational Linguistics (Volume 1: Long Papers)*, 2577–2586. Stroudsburg, PA, USA: Association for Computational Linguistics.
- Johnson, A. E. W.; Pollard, T. J.; Berkowitz, S. J.; Greenbaum, N. R.; Lungren, M. P.; Deng, C.-y.; Mark, R. G.; and Horng, S. 2019. MIMIC-CXR, a de-identified publicly available database of chest radiographs with free-text reports. *Scientific Data*, 6(1): 317.
- Li, C. Y.; Hu, Z.; Liang, X.; and Xing, E. P. 2018. Hybrid retrieval-generation reinforced agent for medical image report generation. In *Advances in Neural Information Processing Systems*, volume 2018-December, 1530–1540.
- Li, C. Y.; Liang, X.; Hu, Z.; and Xing, E. P. 2019. Knowledge-Driven Encode, Retrieve, Paraphrase for Medical Image Report Generation. *Proceedings of the AAAI Conference on Artificial Intelligence*, 33: 6666–6673.
- Lin, C.-Y. 2004. Rouge: A package for automatic evaluation of summaries. In *Text summarization branches out*, 74–81.
- Liu, F.; Wu, X.; Ge, S.; Fan, W.; and Zou, Y. 2021. Exploring and Distilling Posterior and Prior Knowledge for Radiology Report Generation. 13753–13762.
- Lu, J.; Xiong, C.; Parikh, D.; and Socher, R. 2017. Knowing When to Look: Adaptive Attention via a Visual Sentinel for Image Captioning. In *CVPR*.
- Miller, A. H.; Fisch, A.; Dodge, J.; Karimi, A. H.; Bordes, A.; and Weston, J. 2016. Key-value memory networks for directly reading documents. *EMNLP 2016 - Conference on Empirical Methods in Natural Language Processing, Proceedings*, 1400–1409.
- Papineni, K.; Roukos, S.; Ward, T.; and Zhu, W.-J. 2002. Bleu: a method for automatic evaluation of machine translation. In *Proceedings of the 40th annual meeting of the Association for Computational Linguistics*, 311–318.
- Shin, H. C.; Roberts, K.; Lu, L.; Demner-Fushman, D.; Yao, J.; and Summers, R. M. 2016. Learning to Read Chest X-Rays: Recurrent Neural Cascade Model for Automated Image Annotation. *Proceedings of the IEEE Computer Society Conference on Computer Vision and Pattern Recognition*, 2016-December: 2497–2506.
- Vaswani, A.; Shazeer, N.; Parmar, N.; Uszkoreit, J.; Jones, L.; Gomez, A. N.; Kaiser, Ł.; and Polosukhin, I. 2017. Attention is all you need. In *Advances in Neural Information Processing Systems*, volume 2017-December, 5999–6009.

- Vedantam, R.; Lawrence Zitnick, C.; and Parikh, D. 2015. Cider: Consensus-based image description evaluation. In *Proceedings of the IEEE conference on computer vision and pattern recognition*, 4566–4575.
- Vinyals, O.; Toshev, A.; Bengio, S.; and Erhan, D. 2015. Show and tell: A neural image caption generator. In *CVPR*.
- Wang, X.; Peng, Y.; Lu, L.; Lu, Z.; and Summers, R. M. 2018. TieNet: Text-Image Embedding Network for Common Thorax Disease Classification and Reporting in Chest X-Rays. In *Proceedings of the IEEE Computer Society Conference on Computer Vision and Pattern Recognition*, 9049–9058.
- Wu, Z.; Xiong, Y.; Yu, S. X.; and Lin, D. 2018. Unsupervised Feature Learning via Non-parametric Instance Discrimination. *Proceedings of the IEEE Computer Society Conference on Computer Vision and Pattern Recognition*, 3733–3742.
- Xu, K.; Ba, J.; Kiros, R.; Cho, K.; Courville, A.; Salakhudinov, R.; Zemel, R.; and Bengio, Y. 2015. Show, Attend and Tell: Neural Image Caption Generation with Visual Attention. In *ICML*.
- Xue, Y.; Xu, T.; Rodney Long, L.; Xue, Z.; Antani, S.; Thoma, G. R.; and Huang, X. 2018. Multimodal recurrent model with attention for automated radiology report generation. In *MICCAI 2018*, volume 11070 LNCS, 457–466. Springer International Publishing. ISBN 9783030009274.
- Yuan, J.; Liao, H.; Luo, R.; and Luo, J. 2019. Automatic Radiology Report Generation Based on Multi-view Image Fusion and Medical Concept Enrichment. In *MICCAI 2019*, volume 11769 LNCS, 721–729. ISBN 9783030322250.
- Zhang, Y.; Wang, X.; Xu, Z.; Yu, Q.; Yuille, A.; and Xu, D. 2020. When Radiology Report Generation Meets Knowledge Graph. *Proceedings of the AAAI Conference on Artificial Intelligence*, 34(07): 12910–12917.
- Zhou, S. K.; Greenspan, H.; Davatzikos, C.; Duncan, J. S.; Van Ginneken, B.; Madabhushi, A.; Prince, J. L.; Rueckert, D.; and Summers, R. M. 2021. A review of deep learning in medical imaging: Imaging traits, technology trends, case studies with progress highlights, and future promises. *Proceedings of the IEEE*.
- Zhou, S. K.; Rueckert, D.; and Fichtinger, G. 2019. *Handbook of medical image computing and computer assisted intervention*. Academic Press.